Available online at www.sciencedirect.com
SCIENCE DIRECT®
Journal of Nuclear Materials 343 (2005) 81–91
journal of nuclear materials
www.elsevier.com/locate/jnucmat

Benchmarking dynamic strain predictions of pulsed mercury spallation target vessels

B.W. Riemer *

Spallation Neutron Source[1] *Oak Ridge National Laboratory 701 Scarboro Road Oak Ridge, TN 37831, USA*

Abstract

Pulsed mercury spallation targets like that used in the Spallation Neutron Source (SNS) feature a target vessel that strains with each burst of protons. A robust simulation method for predicting the strain response of the target vessel is needed to evaluate the target's fatigue life. The interaction of pressure waves in the mercury with the vessel is a complex problem made more difficult by cavitation. The importance of benchmarking simulations had been recognized by SNS and its R&D program included experiments for measuring strains in various mercury-filled targets responding to single-beam pulses. Recent progress with simulations is reported. Results for two experimental targets are presented and compared to their test data, and the development of simulation parameters improved predictions is discussed. Overall the recent simulations do a fairly good job of predicting strain magnitude and dynamic response. In some target locations the predictions match data quite well, but this quality is not universally achieved.
Published by Elsevier B.V.

1. Introduction

The Spallation Neutron Source (SNS) target vessel (Fig. 1) contains mercury flowing at 23 l/s and is designed to meet structural design criteria considering several mechanical, pressure and thermal loads. Pressure pulses that arise from the rapidly deposited proton beam energy dynamically strain the vessel. This fatigue loading must be considered in the design of the target, but robust methods to estimate the pressure pulse-induced strain have been lacking.

The SNS R&D program included experimental work to measure strain response on test targets hit with single pulses [1]. In itself a technical challenge, the data obtained from these experiments provided a basis for benchmarking and improving simulation techniques to be used on the SNS target. The principal simulation tool used here has been the finite element code ABAQUS/Explicit [2]. The tool itself is not as important as having an appropriate description of mercury behavior and its interaction at the vessel wall interface.

Strain data from targets tested at the Los Alamos Neutron Science Center – Weapons Neutron Research (LANSCE – WNR) facility have dynamic characteristics that are slower than one expects from wave propagation theory. Over the course of the R&D program it became evident that the major strain response is in fact due to the fluid – structure system being excited by an impulsive load. Even then, typical test target dynamics have been slower than expected compared to simulations using nominal mercury properties. It is believed this slow behavior is due to cavitation in the mercury that leads

[1] SNS is managed by UT-Battelle, LLC, under contract DE-00OR22725 for the US Department of Energy.

* Tel.: +1 865 574 6502; fax: +1 865 574 6080.
E-mail address: riemerbw@ornl.gov

0022-3115/$ - see front matter Published by Elsevier B.V.
doi:10.1016/j.jnucmat.2005.01.026

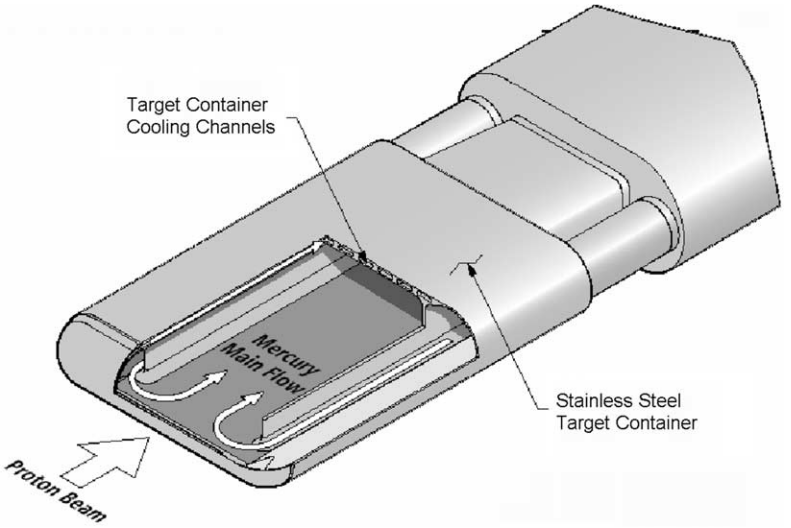

Fig. 1. SNS mercury target vessel.

to a population of bubbles. This bubble mixture can have dramatically different compressibility and attenuation characteristics compared to mercury alone. Very small gas volume fractions in a bubbly mixture can reduce wave speed an order of magnitude.

The bubble population in a mercury spallation target likely varies in size, time and location during the period between pulses, but as yet only limited direct observations of this have been made [3]. In principle, if this population data were known one could model bubble compressibility, attenuation and scattering effects while simulating the strain response of the target [4]. This is a difficult task. The approach taken here has been to develop simulations using empirical models for mercury behavior that predict vessel strains as well as possible.

Described here is recent progress in benchmarking simulations against experimental data from the R&D program. Strain data from two types of test targets are used for a comparison basis: large effects (LE) target data obtained in the July 2001 WNR test campaign, and prototypic shape (PS) target data from the WNR August 2000 tests.

2. Simulation approach

2.1. Analysis code

The explicit version of ABAQUS is employed for these simulations as it has advantages over the implicit version for dynamic analysis of short time scale events especially including contact interaction. Explicit codes also have lower computation memory demand for problems with many degrees of freedom which is an important advantage that will be needed for detailed simulations of the SNS target.

2.2. Material model for mercury

Material models available in ABAQUS that have been tried for mercury were the acoustic media and equation of state (EOS) options. User-written material subroutines based on the EOS model have also been tried with limited success. Both the acoustic and EOS models are appropriate for liquid mercury from the perspective they describe only the volumetric behavior. While the acoustic approach has the advantage of fewer degrees of freedom in the simulation (pressure only) its inherent small perturbation assumptions do not properly relieve the pulse-induced pressure as the vessel expands during its response. Pressure induced by the proton beam in these targets is high relative to acoustic phenomena: the order is of tens of MPa. However, this is low compared to explosive or shock events.

The EOS option is displacement/strain based and thus accounts for volume changes of the material. Here in ABAQUS the Mie-Gruneisen option is selected and mercury's initial density and wave speed are specified at $\rho_0 = 13\,500\ \mathrm{kg/m^3}$ and $c_0 = 1456\ \mathrm{m/s}$. As no true shock phenomena are involved the Gruneisen constant Γ_0 and particle speed coefficient S are set to zero. Early trial solutions confirmed insensitivity to these parameters.

Under these conditions the EOS model reduces to a simple relation between pressure and volumetric strain:

$$P = \rho_0\ c_0^2 \eta, \tag{1}$$

where $\eta = 1 - \rho_0/\rho$ is the nominal volumetric compressive strain (ρ is the density as a function of solution time); $\rho_0 c_0^2$ is simply the elastic bulk modulus.

This model is applicable provided there is no cavitation, but there is substantial evidence that cavitation occurs under relevant short-pulse proton beam irradiation [5,6]. The sound speed is very sensitive to the bubble void fraction. Consider the simple case for sound propagating through a bubbly liquid. Minnaert's relation [7] for low-pressure regimes where the sound frequency is below resonant bubble frequencies has been verified by experiment (for example, see [8, Chapter 6]). It shows the remarkable feature that the mixture wave speed can be much smaller than either of its constituents. Applied to mercury–helium bubble mixtures the predicted wave speed as a function of helium void fraction is shown in Fig. 2. The speed has dropped by a factor of 10 at only 0.035% void; this is equivalent a bulk modulus reduction of 100.

Granted, the bubble population during a pulse is not known and the applicability of Minnaert's relation to spallation target conditions is questionable, but the order of the reduction with small void fractions suggests that employing negligible bulk stiffness when cavitation occurs is not wildly unrealistic. This behavior can be implemented in ABAQUS with the EOS model by using a tensile failure option. At a specified cavitation threshold (cutoff pressure) all volumetric stiffness is lost; it can be recovered if the material is compressed to strain levels corresponding to this pressure. A similar approach had been tried by others including Ni [9]. Put in acoustic terms, failed material acts an as impedance barrier.

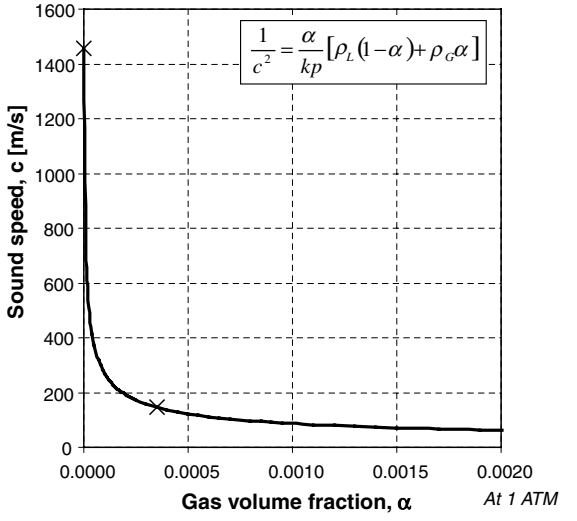

Fig. 2. Sound speed as a function of bubble void fraction, per Minaert [7].

When pressure returns above the cutoff pressure the nominal wave speed is restored.

The threshold of cavitation was a key parameter of this benchmark work. Experimental work done on cavitation threshold in mercury with representative levels of helium saturation [10,11] indicated the practical onset of cavitation occurs at only a few bar tensile pressure in contrast to theory [12] or extreme experimental controls [13]. Low-threshold values provided a starting point for these recent simulations studies.

2.3. Mercury–vessel interaction

The interaction between the mercury and vessel wall is difficult to understand without relevant experimental observations, let alone model. Previous simulation efforts by the author investigated various contact behavior such as penalty stiffness, contact damping and non-separating sliding contact options. These features add complexity to the solutions, and the present assessment is that they provide little value. Benchmark cases presented here use 'tied' contact that bonds the interface in both normal and transverse directions. The rationale is that any cavitation that occurs at the interface will be accounted for by the mercury failure model.

2.4. Bulk viscosity/numerical damping

Another parameter of interest in the simulations is bulk viscosity, an ABAQUS term for damping associated with volumetric straining. Its intended purpose is to improve the numerical modeling of high-speed dynamic events. ABAQUS/Explicit contains two forms of bulk viscosity: linear and quadratic. The quadratic form is intended for shock problems to prevent element collapse under severe compression; experience has shown it has no significant influence on target pressure pulse problems. Linear bulk viscosity is introduced to damp ringing in the highest element frequency. This damping is sometimes referred to as truncation frequency damping. It generates a bulk viscosity pressure that is linear in the volumetric strain rate:

$$p_{bv1} = b_1 \rho c_d L_e \dot{\varepsilon}_{vol}, \tag{2}$$

where b_1 is a damping coefficient (default = 0.06), c_d is the current dilatational wave speed, L_e is an element characteristic length, and $\dot{\varepsilon}_{vol}$ is the volumetric strain rate.

In earlier simulations the amount of bulk viscosity was drastically reduced from the default amount because the amount of energy lost from this numerical conditioning was large in comparison to strain and kinetic energies in the simulation. There was no basis to believe this degree of damping represented some physical effect. However, low-bulk viscosity leads to noisy strain predictions.

2.5. Target vessel material behavior

Test target vessels were constructed primarily from type 304L stainless steel. A simple elastic material description was used with a modulus of elasticity of 195 GPa and density of 8000 kg/m^3. Measured strains were generally well below the elastic limit. The exception was the end flanges of the LE targets. These were made of type 316LN stainless steel with a slightly lower modulus. In addition the flanges had been fully annealed. Measured strains were right at the elastic limit for the flanges, so an elastic-plastic material definition was used for the simulations. The elastic limit in the material description was at 1340 micro-strain (or 259 MPa). Linear thermal expansion is defined as 15.8×10^{-6}/K for both types of steel. A small amount of material stiffness damping is also included.

2.6. Deposited energy pressure application

The pressure pulse is defined in the simulation by initial, non-equilibrium pressure conditions spatially defined in the mercury based on energy deposition data [14]. The energy data is converted to pressure by

$$\mathrm{d}P = Q \cdot \frac{\beta K}{\rho C_V}, \tag{3}$$

where

$\mathrm{d}P$	pressure rise [Pa];
Q	volumetric energy deposition [J/m^3];
β	mercury volumetric expansion coefficient = 183×10^{-6} K;
K	mercury bulk modulus of elasticity = 28.6 GPa;
ρ	mercury density = 13 500 kg/m^3;
C_v	mercury constant volume specific heat = 140 J/kg K.

Using instant application is based on the fact that heat transfer and inertial response are insignificant in the time scale of the beam pulse. Similarly, temperatures in the steel vessel can be defined based on adiabatic conditions and applied as a step input. Previous simulations that included the temporal profile of the beam pulse did not produce different results and it is easier to use instantaneous loading.

2.7. Simulation time

These benchmark simulations typically cover a 5 ms time period. Two analysis steps were usually defined. During the first step (10 μs) the analysis time increment is scaled to one half its nominal value to provide an extra stability margin. Thereafter, the time increment is not scaled. The increment is calculated by ABAQUS and is based on the smallest transit time of a dilatational wave across any of the elements in the mesh, which is typically determined by the smallest steel vessel element.

3. WNR test conditions

WNR beam test parameters are summarized in Table 1 along with those from SNS for comparison. The main

Table 1
WNR test beam parameters, SNS beam parameters

	WNR	SNS (at 2 MW)
Proton energy [GeV]	0.8	1
Protons per pulse	2.8×10^{13}	2×10^{14}
Beam size [mm]	Circular, $\sigma \sim 10$	Elliptic, $\sim 70 \times 200$
Energy deposited in mercury target [kJ]	2.1	20
Maximum energy deposition density [MJ/m^3]	19	13
Peak initial pressure [MPa]	50	36
Pulse frequency [Hz]	Single pulses	60

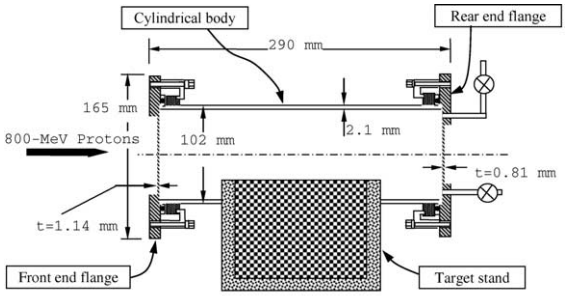

Fig. 3. Large effects target dimensions.

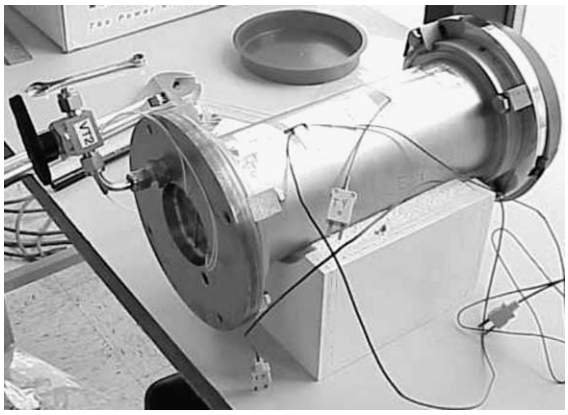

Fig. 4. Large effects target in preparation for test.

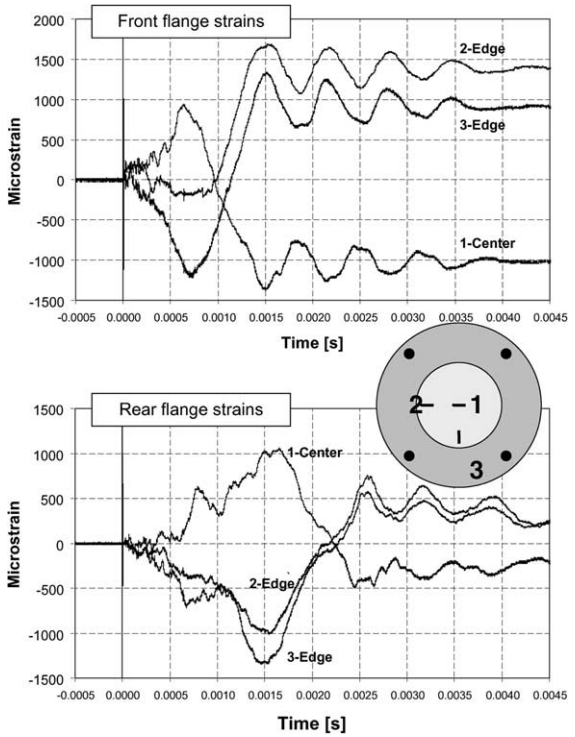

Fig. 5. Typical measured strains from front and rear flanges of LE target.

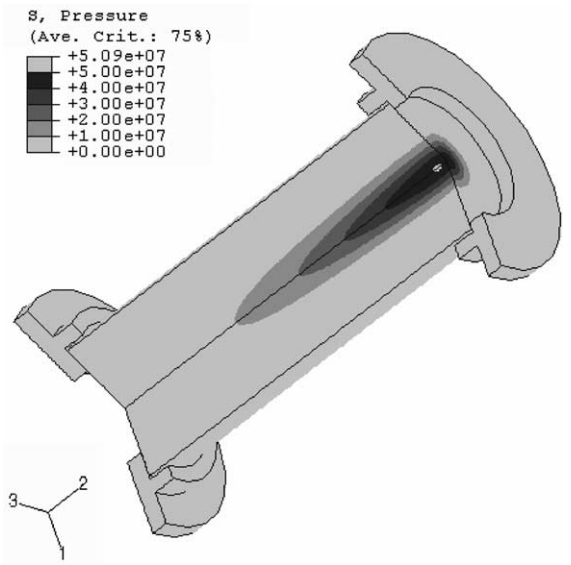

Fig. 7. Initial pressure in LE target from WNR beam pulse [Pa].

advantages of this combination of test beam and target were that proton energy, beam size to target size proportion, and peak energy density (i.e., peak initial pressure) are similar to a 2 MW SNS pulse. Beam repetition rate was limited at the WNR to one pulse per minute. Test targets were also lacking in some prototypic features such as flowing mercury.

3.1. Large effects targets

The large effects (LE) targets tested at the WNR are axisymmetric in shape. Fig. 3 shows LE dimensions as configured for the July 2001 WNR test. The end flanges were machined at the center to form membrane regions that provided for significant strain response. The cylindrical body is a standard vacuum nipple component. The end flanges are type 316LN stainless steel, the type to be used in the SNS target front end. Since these particular tests were also used for studying vulnerability to cavitation pitting damage, the flanges were also annealed. Targets rested on wood and Styrofoam saddle stands during test. A photograph of a target is shown in Fig. 4.

Two similar LE targets were hit with 200 pulses each during the July 2001 test, and altogether, strain data was collected for about 100 pulses. Time capture varied from 1 to 100 ms; the data were generally consistent pulse to pulse. Strain from a typical 5 ms data capture is shown in Fig. 5. Three strain gauges on both the front and rear membranes were oriented as shown on the accompanying graphic in Fig. 5. The data show the edge strains moving in unison with each other and opposite to the center; this indicates an axisymmetric response. Some difference between front edge strains is evident, but edge gauge 2 apparently is not responding well for the initial 1 ms and the difference may be related to this. Front

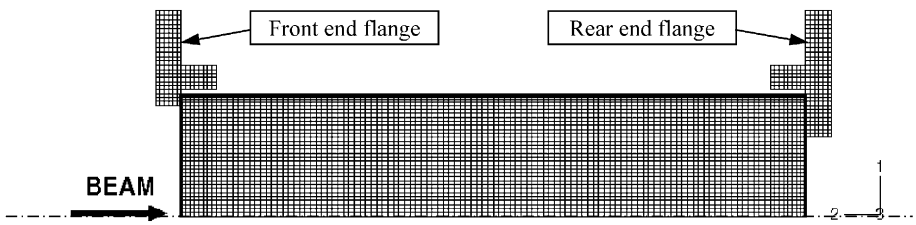

Fig. 6. Large effects target axisymmetric model.

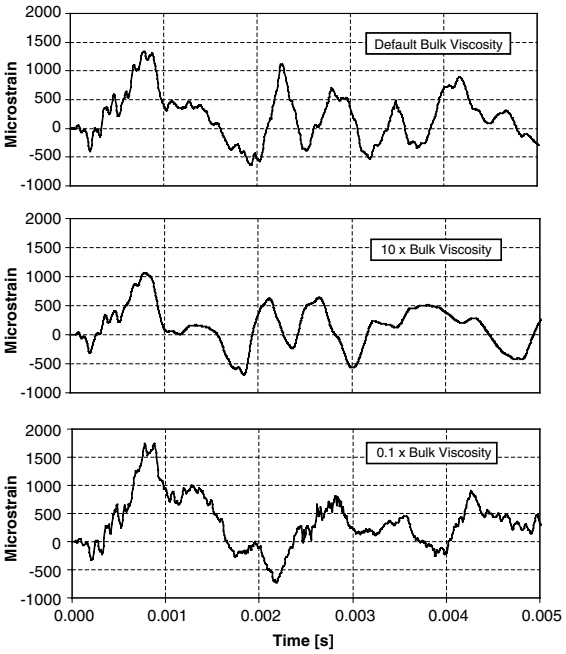

Fig. 8. Predicted rear center strain with changing bulk viscosity. Cavitation threshold employed was 0.3 MPa.

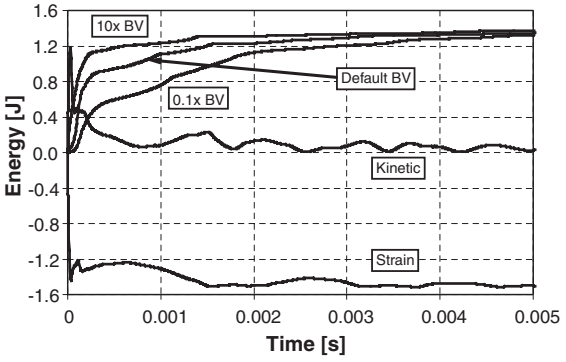

Fig. 9. Predicted mercury energies. Accumulated damping associated with bulk viscosity (BV); strain and kinetic energies with default BV.

strains reach magnitudes around the elastic limit, it is not clear that yielding occurs.

Two-dimensional, axisymmetric simulations of the LE target allowed for many iterations of modeling conditions to help find the best solution parameter values. The axisymmetric model is shown in Fig. 6. It uses shell type elements for the target flange membranes as well as the cylindrical wall. Thick flange sections and the mercury are done with continuum elements. The initial pressure is shown in Fig. 7.

The benchmark simulations began with mercury modeled as described above and the cavitation threshold set at 0.3 MPa. Results were promising in that predicted

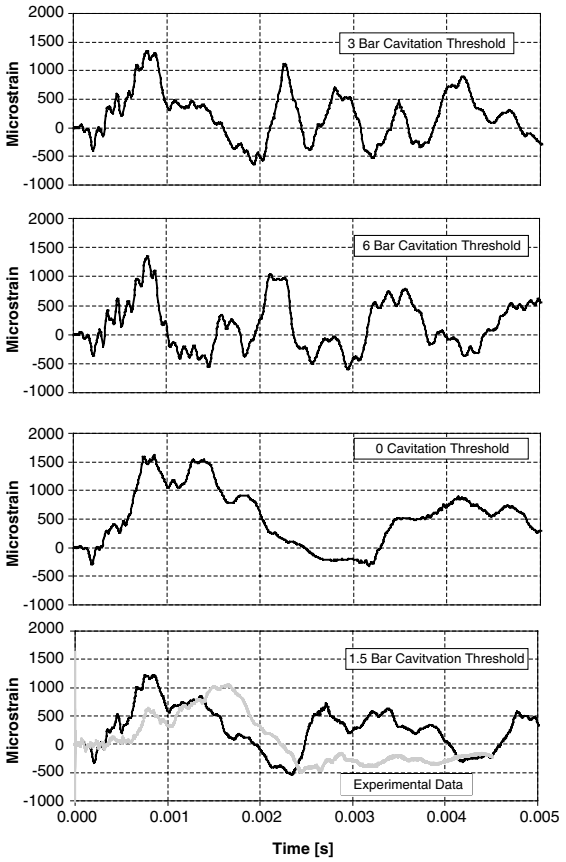

Fig. 10. Predicted rear center strain with changing cavitation threshold. Default bulk viscosity employed.

strain magnitudes and major dynamic frequencies were more comparable to the test data than earlier attempts. The first parameter varied to look for improvement was bulk viscosity. However, changing the linear bulk viscosity by factors of ten did not substantially improve major frequencies and strain magnitudes. Fig. 8 shows the predicted strains for the rear center location as an example. Aside from effecting high-frequency content in the predicted strains, the bulk viscosity altered the initial peak strain. Higher damping gave a somewhat better magnitude match but dynamic character was generally not improved.

Fig. 9 shows energy lost to bulk viscosity damping for these three cases along with mercury strain and kinetic energies under the default bulk viscosity condition. By 5 ms the energy lost to damping is the same for each case. The main difference is how fast the damping initially acts. Also note that the accumulated damping energy is close in magnitude to the strain energy and initial kinetic energy. Nevertheless, the concern regarding large relative damping due to bulk viscosity was put aside and the default bulk viscosity was used from here forward.

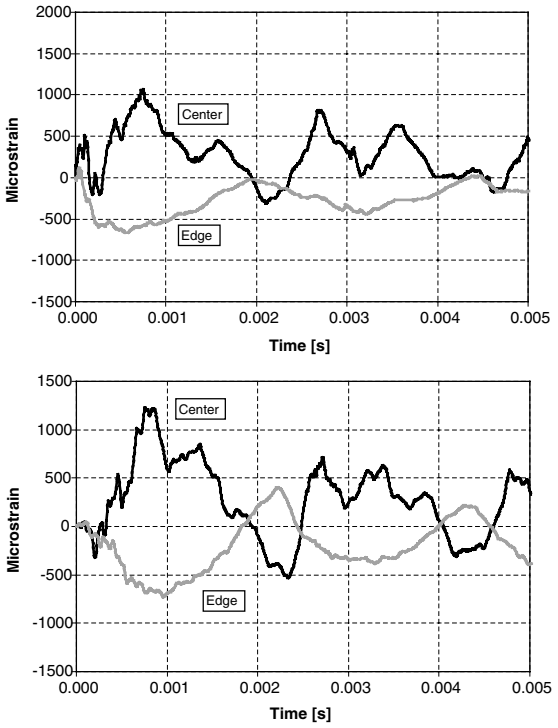

Fig. 11. Predicted front and rear strains with 0.15 MPa cavitation threshold and default bulk viscosity.

Fig. 12. Prototypic-shape target with strain sensors.

The cavitation threshold was investigated next, with 0, 0.3, 0.6 and 0.15 MPa tensile pressures attempted. The result is shown in Fig. 10 for the rear center location. The experimental data is also included for comparison. This parameter showed surprising influence on the major frequencies of predicted strain considering the

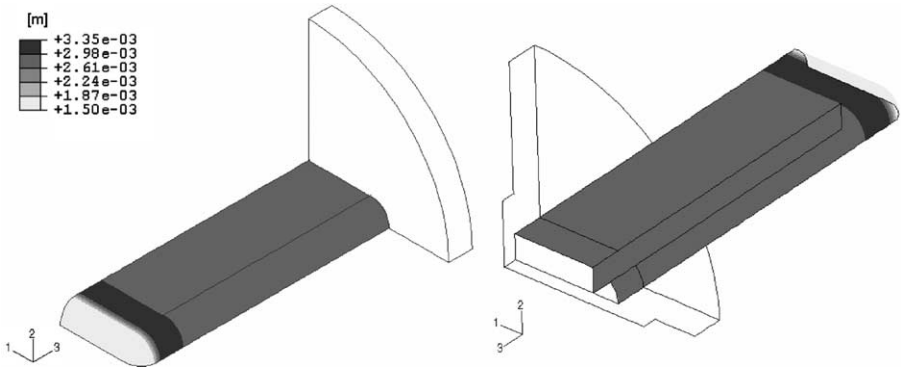

Fig. 13. Prototypic shape target 1/4 symmetry model vessel wall thickness.

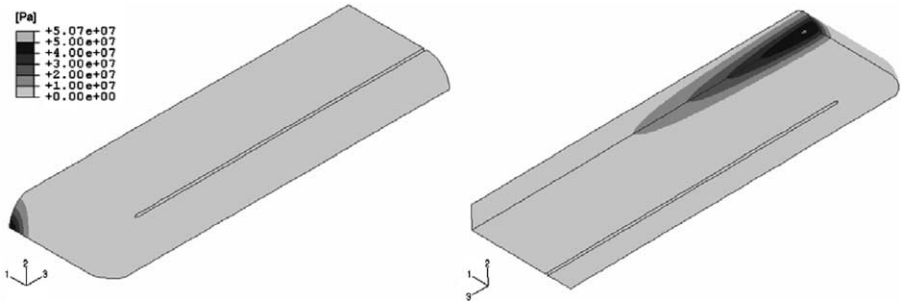

Fig. 14. Prototype shape target 1/4 symmetry model mercury initial pressure.

initial pressure magnitude is 50 MPa. Although the match to the experimental data was still less than desired, the best overall agreement was judged to be at 0.15 MPa. Predicted strains for all front and rear locations are shown in Fig. 11 for comparison to the data in Fig. 5.

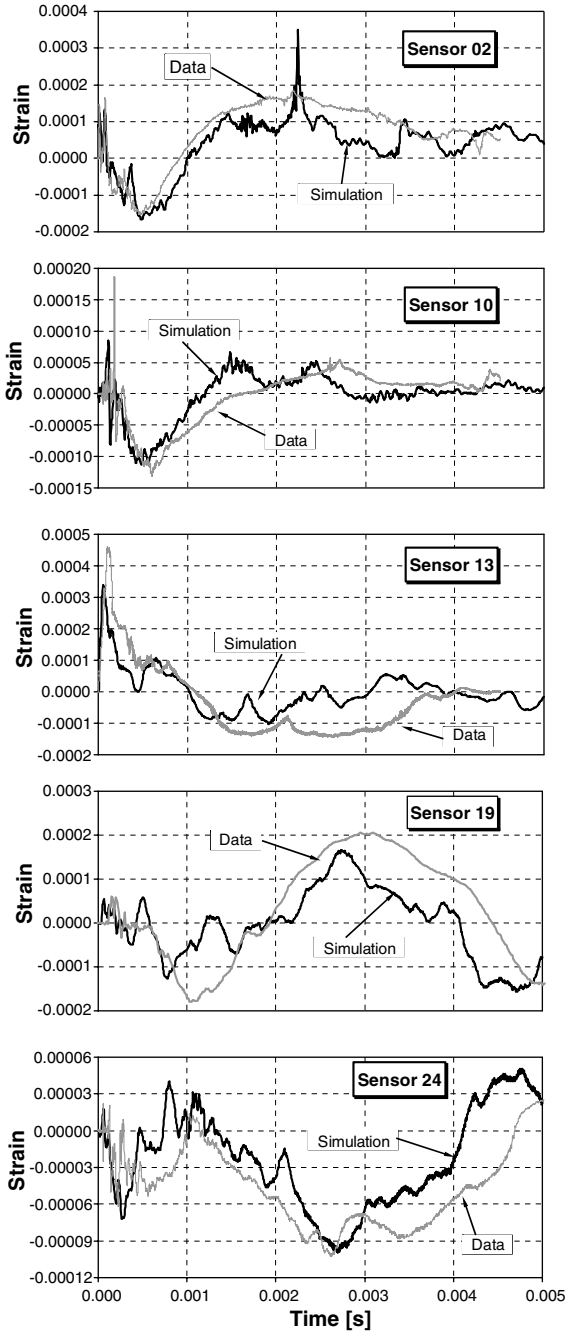

Fig. 15. Predicted and measured strains for PS target.

While this result was better than previous (unpublished) simulations, the match to experiment is still lacking in several aspects. The experimental data features large swings in sign at 1 ms in the front and after 2 ms in the rear that are not predicted; initial edge location peaks are under predicted; the rear initial peaks occur early compared to the data. The strain data relative phase suggests a mode of response that moves membranes in the same direction together, but simulation strains indicate a different mode with movement in opposite directions.

Attempts to improve on this were unproductive. One concern was that although EOS behavior does not include shear stiffness, it was conceivable that the volumetric stiffness could impose shear constraints at the interface that unrealistically influence the results. This was examined by changing the interface condition between mercury and vessel to a sliding, non-separating condition. Essentially the same strains were predicted as for the tied interface, and completing 5 ms of simulation time was more difficult due to hourglass stability problems not present with the tied interface. Another series of three-dimensional model simulations was done to include the stand and gravity, but these too failed to make improvement in matching the magnitude and dynamic character of the experimental data. Even this simple axisymmetric shape was not accurately modeled.

3.2. Prototypic shape targets

During the August 2000 WNR test campaign two prototypic shape (PS) targets were tested. Beam conditions and internal target configurations were altered to study different effects, but generally the same beam condition was used as described for the LE targets in the preceding section. A useful body of strain data was collected [15]. Data was reproducible and consistent. Strain magnitudes scaled linearly with the number of protons per pulse.

PS targets featured internal baffles similar to the SNS target as well as a relatively thin beam window. The main bodies were constructed from type 304L stainless steel using $51 \times 152 \times 3$ mm rectangular tubing with 51×3 mm diameter tube halves welded on each side. Target nose sections were machined from block material to provide a single thin wall for the beam window that was nominally 1.5 mm thick. The overall length to the back flange was 305 mm. A photograph of one of the PS targets is shown in Fig. 12.

A quarter section, 3D finite element model of the PS target was developed using shell elements for the vessel walls and baffle and continuum elements for the mercury and back flange. As-built thicknesses were incorporated into the simulation model and are shown on the model in Fig. 13. The target vessel was modeled with purely elastic behavior. Mercury was modeled with the EOS

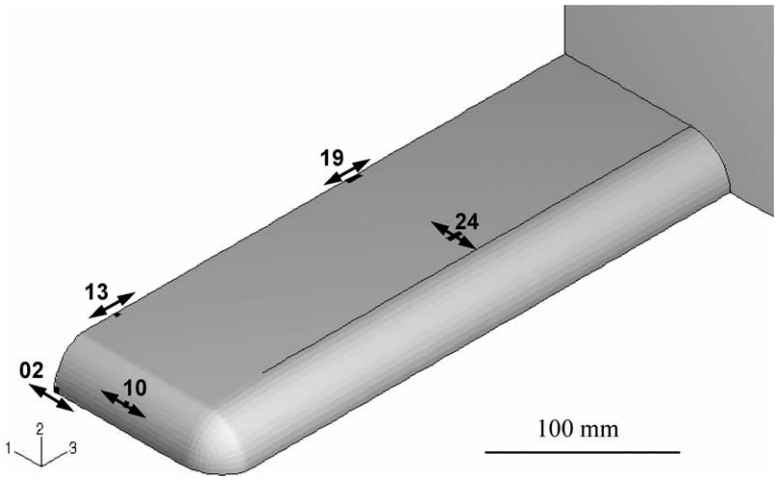

Fig. 16. Example sensor locations and orientations on PS target.

material model with a 0.15 MPa cavitation threshold and default bulk viscosity and was tied to the vessel wall. The initial mercury pressure field imposed by the WNR beam is shown in Fig. 14.

Overall, the simulation parameters developed for the LE target worked better for the PS target. Some comparison examples are shown in Fig. 15. These test targets were instrumented with 25 strain sensors and the locations of those used in the examples are shown in Fig. 16. In many cases the simulation matches both the magnitude and dynamics well. The quality of the PS experimental data is good but it does vary with location and test series. Not shown here are other locations where the match is not as good and a few where it is poor. For these worst locations the simulation strain peaks are off by no more than a factor of two from the experiment. It is not clear how much is due to simulation technique, data problems or experiment conditions.

4. Discussion

These simulations show progress in simulation technique, especially with the prototype target test data. It is still not at a level that can be called robust, but for the time being this approach will be used in simulations in support of the SNS target design. The value in matching experimental data cannot be overstated.

While predicting strain to within a factor of two is good progress for simulation technique it is not especially good for evaluating fatigue life. At high cycles the fatigue design curve is flat or nearly flat (i.e., an endurance limit). The estimated strain could be under the curve by a small margin thus suggesting an infinite fatigue life, but the uncertainty in the estimate must be considered in the safety factor for fatigue life evaluation.

Despite the lack of justification for damping, the latest simulations have shown the default bulk viscosity to give the best comparison to measured strains. It is speculated that the bulk viscosity is fortuitously accounting for damping associated with bubbles. A population of the right size and density of bubbles would significantly dampen pressure waves [16,17].

The Alternating Gradient Synchrotron Spallation Target Experiment (ASTE) collaboration included strain measurements on a mercury-filled target vessel. Good agreement has been reported with experimental data [18] for the ASTE target when hit with 24 GeV AGS proton beam pulses. It is believed that the predominant response for this target/beam condition is stress wave propagation in the steel vessel from direct heating of the steel, rather than mercury pressure driving the vessel response. This large cylindrical target with hemispherical beam window is relatively stiff to the pressure pulse induced by the AGS beam. This is a significant difference to the LE and PS targets tested at the WNR, and it is not the expected condition for high-powered spallation targets. Conversely, the LE target errs in the opposite direction with strains much higher than allowable in a practical spallation target.

The fact that simulation LE strains do not match as well as for the PS may not be as detrimental considering those targets have higher than prototypic strain levels. However, another non-prototypic feature may overwhelm these considerations entirely: beam repetition rate. The SNS will operate at 60 Hz leaving little time for cavitation-induced bubbles to dissolve, condense, rise to the surface or be carried away by flow. Pre-existing bubbles were not a condition present in the WNR tests; it may be that they mitigate, or at least alter, the effects of the pressure pulse. There is no experimental strain data available with a sufficiently prototypic

repetition rate to benchmark simulations in this regime.

Deliberate bubble injection has been a feature of the European Spallation Source target as a technique to mitigate beam pressure magnitudes that are substantially higher than SNS. SNS is now interested in bubble injection as a means to mitigate cavitation pitting damage, and the technology is being developed under an international collaboration. If the technology becomes completely successful in mitigating pressure-pulse induced stresses there would be little need for improved simulation methods.

Short of this optimistic scenario, efforts to improve simulations will continue. While it is possible to include physics of bubble dynamics in sophisticated analysis software, without benchmarking to relevant experimental data the credibility of such simulations should be questioned.

5. Conclusion

Recent simulations of the structural response of mercury filled vessels hit with short, intense proton pulses have shown improvement in predicting strain magnitude and dynamics. The main difficulty has been including the effects of cavitation in the mercury. A simple approach was employed to fail the mercury at a specified level of tensile pressure, or cavitation threshold. In a series of benchmark simulations for the LE targets tested at the LANSCE-WNR it was found that the predicted strains were very sensitive to this cavitation threshold value. Adjusting the tensile failure between zero and 0.6 MPa greatly changed the predicted dynamic response of the vessel. This was surprising considering initial beam pressure levels reach 50 MPa. A value of 0.15 MPa gave the best match to the data.

The predicted dynamic character of strains for the LE target was better than previously achieved but still did not match the data well. Simulation of the PS target using parameters developed for LE did a better job of matching experimental data. Predicted strains at many locations are a good match both in magnitude and dynamic character to experimental data. At locations where the match is not good, the magnitude is either over predicted or underestimated by no more that a factor of two. Strain levels in the PS target are more prototypic to the SNS target than are LE strains, so the better benchmark comparison is encouraging for use on SNS simulations.

A potentially significant factor in strain simulation technique is accounting for pre-existing bubbles. At high-beam repetition rates, a condition not part of the experimental data, bubbles are more likely to persist between pulses. There is reason to believe such bubbles could mitigate target vessel strains, but this remains to be demonstrated.

Acknowledgements

The author extends his gratitude to Tony Gabriel, John Haines, Dave Lousteau, and Tom McManamy of SNS Target Systems for their leadership, support and patience throughout the course of this work. Contributions from Kurt Moesslacher, now of the Northrop Grumman Corporation, included running many simulation cases for the author. The experimental strain data used for this benchmarking is especially valuable and was obtained via an SNS R&D program supported by many both within and outside of the project. Special thanks go to Mike Cates, Duncan Earl, and Jim Tsai (ORNL); Steve Wender, Bruce Takala, Gregg Chaparro (LANL); Harald Conrad (Forschungszentrum Jülich) and Kenji Kikuchi (Japan Atomic Energy Research Institute).

References

[1] J.R. Haines, D.K. Felde, B.W. Riemer, C.C. Tsai, M.W. Wendel, Final report on mercury target development, ORNL/SNS 101050000-TR0001-R00, 2003.
[2] ABAQUS/Explicit, Version 6.3, ABAQUS, Pawtucket, Rhode Island.
[3] M.R. Cates, Detection of voids in liquid mercury during 800 MeV proton bombardment, ORNL/SNS-101060100-TR0007-R00, 2002.
[4] S. Ishikura, J. Nucl. Mater. 318 (2003) 113.
[5] B.W. Riemer, J. Nucl. Mater. 318 (2003) 92.
[6] J.D. Hunn, J. Nucl. Mater. 318 (2003) 102.
[7] M. Minnaert, Philos. Mag. 16 (1933) 235.
[8] C.E. Brennen, Cavitation and Bubble Dynamics, Oxford University Press, NY, 1995.
[9] L. Ni, G.S. Bauer, J. Pressure Vessel Technol., ASME 120 (1998) 359.
[10] R.P. Taleyarkhan, F. Moraga, C.D. West, Experimental determination of cavitation thresholds in liquid water and mercury, in: Proceedings of the 2nd International Meeting on Nuclear Applications of Accelerator Technology (AccApp '98), Gatlinburg, TN, Am. Nucl. Soc., 1998.
[11] F. Moraga, R.P. Taleyarkhan, Static & transient cavitation threshold measurements for mercury, in: Proceedings of the 3rd International Topical Meeting on Nuclear Applications of Accelerator Technology (AccApp '99), Long Beach, CA, Am. Nucl. Soc., 1999.
[12] C.D. West, Cavitation in a mercury target, ORNL/TM-2000/263, 2000.
[13] L. Briggs, J. Appl. Phys. 24 (4) (1953) 488.
[14] P. Ferguson, Unpublished results of MCNPX calculation, 800 MeV proton heating-large effects.xls,l MS-Excel summary (SNS).

[15] M.R. Cates, Strain measurements on targets tested at the LANSCE-WNR facility August 2000, ORNL/SNS 101050200-TR0009-R00, July 2001.
[16] H. Soltner, Gas bubble admixture for pressure pulse mitigation in high-power liquid-mercury spallation targets, ESS 03-152-T, Forschungszentrum Jülich, 2003.
[17] H. Soltner, Effects of gas bubble admixture on pressure pulse propagation in liquids, ESS 03-153-T, Forschungszentrum Jülich, 2003.
[18] H.C. Conrad, C. Byloos, Stress wave experiments with the ASTE target, Presentation at 7th General ESS Meeting, Seggau, Austria, 2002.